Available online at www.sciencedirect.com
ScienceDirect
Journal of Sound and Vibration 323 (2009) 609–625
JOURNAL OF SOUND AND VIBRATION
www.elsevier.com/locate/jsvi

A new experimental method to estimate viscoelastic properties from ultrasonic wave transmission measurements

K. Fujisawa[1], Y. Takei*

Earthquake Research Institute, University of Tokyo, 1-1-1, Yayoi, Bunkyo-ku, Tokyo 113-0032, Japan

Received 2 September 2007; received in revised form 25 December 2008; accepted 8 January 2009
Handling Editor: L.G. Tham
Available online 25 February 2009

Abstract

We develop a new experimental method to estimate viscoelastic properties of a sample by ultrasonic wave transmission. Viscoelastic properties are generally described by the frequency dependent phase velocity $v(f)$ and the quality factor $Q(f)$. In order to estimate $v(f)$ and $Q(f)$ from waveform data obtained by the ultrasonic wave transmission method, it is necessary to correct the data for the effects of dynamic response of the source and receiver transducers and of the wave diffraction caused by finite size source. A practical method to perform these corrections based on the theoretical models is developed. The validity of the present method is demonstrated by applying it to the experimental data for stainless steel sample ($Q \gg 200$), acrylic plastic sample ($Q \sim 100$), and partially molten organic polycrystal sample ($Q < 10$). In comparison with the other existing methods, the present method has the advantage of not requiring any reference waveform. Using the results of this study, we discuss the validity of the reference method.
© 2009 Elsevier Ltd. All rights reserved.

1. Introduction

Ultrasonic wave transmission method using piezoelectric transducers has been frequently used for estimating sample acoustic properties [1–3], for non-destructively monitoring microstructural evolution [4,5], and for simulating elastic wave propagation in heterogeneous media [6]. In this method, the obtained waveform data are influenced not only by the acoustic behavior of the sample but also by the electro-mechanical behavior of the source and receiver transducers (transducer effect) and by the wave diffraction which is determined by the size of the transducers (diffraction effect). Therefore, in order to know the acoustic behavior of the sample, correction of the data for these two effects is important. Most of our concern in this paper is the estimation of sample acoustic properties, especially the viscoelastic properties which are generally described by frequency dependent phase velocity $v(f)$ and quality factor $Q(f)$. Correction methods used in previous studies were based on the reference waveforms obtained for a standard material with well-known acoustic properties. In the pulse reflectometry methods [7–9], the transducer effect is eliminated by using a

*Corresponding author. Tel.: +81 3 5841 5770; fax: +81 3 5802 3391.
E-mail address: ytakei@eri.u-tokyo.ac.jp (Y. Takei).
[1]Now at Japan Patent Office.

0022-460X/$ - see front matter © 2009 Elsevier Ltd. All rights reserved.
doi:10.1016/j.jsv.2009.01.016

reference waveform, which propagates a buffer rod, and the diffraction effect is eliminated by assessing the effect from acoustic theory. In the transmission measurements [10–12], the two effects are eliminated by using a reference waveform, which is obtained by replacing the sample in the experimental assembly by a standard material.

In this study, we develop a new method of the correction for the transducer and diffraction effects by using theoretical models. In comparison with the other existing methods, our method has the advantage of not requiring any reference waveform, and hence can be used for testing the validity of the reference method. Our method is designed to be applicable to transmission measurements. Because the assembly of the transmission measurement is simple, our method can be used widely.

The essential part of our method is the theoretical derivation of the transducer effect and the diffraction effect (Section 2). The dynamic response of the piezoelectric disk attached to an acoustic (zero rigidity) sample was theoretically calculated by Stepanishen [13], based on the formulation of Mason [14] and Seki et al. [15]. We extend the previous studies by taking into account the effect of sample rigidity and the dynamic response of the receiver transducer. We present a practical method which can be immediately used to determine the frequency dependent phase velocity and attenuation from the transmission measurement. In order to test the validity of our method, we conduct an ultrasonic wave transmission experiment on stainless steel, acrylic plastic, and organic polycrystal samples, which are characterized by high, intermediate, and low Q, respectively (Section 3). By using sinusoidal waves and/or narrow band pulses generated by broadband transducers, transfer functions between source and receiver signals are obtained in the frequency domain for 100 kHz–1 MHz. By correcting the data using our method, phase velocity and attenuation are determined for this frequency range.

2. Waveform analysis to estimate frequency dependent phase velocity and quality factor

2.1. Definition and derivation of transducer effect H^T and diffraction effect H^a

We consider a system consisting of a sample and two piezoelectric transducers attached to both sides of the sample (Fig. 1). The sample is assumed to be a linear viscoelastic material represented by phase velocity $v(f)$ and quality factor $Q(f)$ at frequency f. Let V^S and V^R be the voltage signals of the source and receiver transducers, respectively. V^S is applied by a function generator and V^R is measured by an oscilloscope, and hence both V^S and V^R are known. Time series data are written as $V^S(t)$ and $V^R(t)$, and the complex Fourier components are written as $V^S(f)$ and $V^R(f)$. The goal of Section 2 is an accurate estimation of $v(f)$ and $Q(f)$ from $V^S(f)$ and $V^R(f)$.

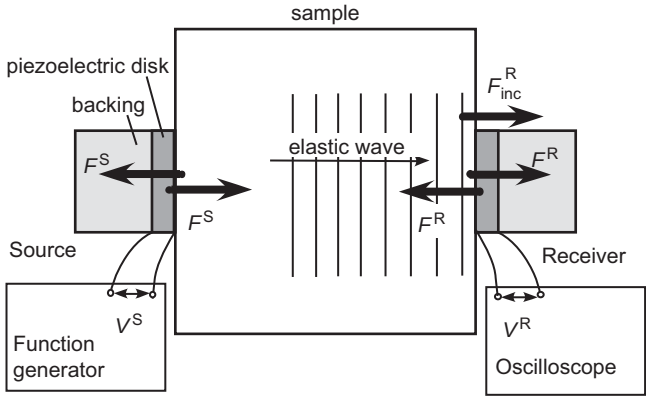

Fig. 1. Schematic illustration of an assembly of transmission measurement using broadband transducers consisting of piezoelectric disk and backing. F and V represent traction and voltage, respectively.

We introduce transfer function H^{obs} defined by

$$H^{\mathrm{obs}}(f) = \frac{V^R(f)}{V^S(f)}. \tag{1}$$

H^{obs} is related to $v(f)$ and $Q(f)$ as

$$H^{\mathrm{obs}}(f) = H^T(f)H^a(f)\exp\left\{-\mathrm{i}\omega\frac{l}{v(f)}\left(1-\frac{\mathrm{i}}{2Q(f)}\right)\right\}, \tag{2}$$

where $\omega(=2\pi f)$ is angular frequency and l is the sample length. The exponential factor in the right-hand side of Eq. (2) represents the transfer function for plane wave propagation in the sample (e.g. [16]). Because H^{obs} is not simply determined by this exponential factor, but also affected by the dynamic response of the transducers [13] and the diffraction at the finite size source [15], we express H^{obs} in the form of Eq. (2). In order to estimate $v(f)$ and $Q(f)$, H^{obs} should be corrected for transducer effect H^T and diffraction effect H^a. H^T and H^a are derived from theoretical models.

Let F^S and F^R be the tractions at the surface of the source and receiver transducers and let F^R_{inc} be the traction of the wave incident on the receiver transducer. H^{obs} defined by Eq. (1) can be rewritten as

$$H^{\mathrm{obs}} = \frac{V^R}{V^S} = \frac{F^S}{V^S}\frac{F^R_{\mathrm{inc}}}{F^S}\frac{F^R}{F^R_{\mathrm{inc}}}\frac{V^R}{F^R}. \tag{3}$$

The factor F^R_{inc}/F^S in the rightest hand side of Eq. (3) is the transfer function for elastic wave propagation, and the other factors, F^S/V^S, F^R/F^R_{inc}, and V^R/F^R, are determined by the dynamic response of the transducers. Therefore, H^a and H^T introduced in Eq. (2) are defined by

$$H^a\exp\left\{-\mathrm{i}\omega\frac{l}{v(f)}\left(1-\frac{\mathrm{i}}{2Q(f)}\right)\right\} = \frac{F^R_{\mathrm{inc}}}{F^S}, \tag{4}$$

$$H^T = \frac{F^S}{V^S}\frac{V^R}{F^R}\frac{F^R}{F^R_{\mathrm{inc}}}, \tag{5}$$

and H^a and H^T are called diffraction effect and transducer effect, respectively.

In order to derive H^T defined by Eq. (5), dynamic response of a broadband transducer consisting of a piezoelectric disk and a backing is modeled based on the mechanical and electrical governing equations. Detailed formulations are presented in Appendix A. The factor F^S/V^S in the right-hand side of Eq. (5) is calculated by solving Eqs. (A.1)–(A.3), the factor V^R/F^R is calculated by solving Eqs. (A.4) and (A.5), and the factor F^R/F^R_{inc} is given by Eq. (A.7). Finally, H^T is obtained as

$$\begin{aligned} H^T = & -2\varepsilon(z_s/z_0)\frac{(z_b/z_0)(1-\mathrm{i}/(2Q_b))+D^S-C^S}{\{(z_s/z_0)+D^S\}\{(z_b/z_0)(1-\mathrm{i}/(2Q_b))+D^S\}-(C^S)^2} \\ & \times\frac{(z_b/z_0)(1-\mathrm{i}/(2Q_b))+D^R-C^R}{\{(z_s/z_0)+D^R\}\{(z_b/z_0)(1-\mathrm{i}/(2Q_b))+D^R\}-(C^R)^2}, \end{aligned} \tag{6}$$

where z_0, z_s, and z_b represent the acoustic impedances of the piezoelectric disk, sample, and backing, respectively, and Q_b represents the quality factor of the backing. $D^{S,R}$, $C^{S,R}$, and ε are given by

$$\begin{cases} D^S = -\mathrm{i}\{\cot(\pi f/f_r)-\varepsilon\}, \\ C^S = -\mathrm{i}\{\mathrm{cosec}(\pi f/f_r)-\varepsilon\}, \\ D^R = -\mathrm{i}\cot(\pi f/f_r), \\ C^R = -\mathrm{i}\,\mathrm{cosec}(\pi f/f_r), \\ \varepsilon = \dfrac{k_0^2}{\pi(f/f_r)}, \end{cases} \tag{7}$$

where resonant frequency f_r and piezoelectric coupling factor k_0 of the disk are given by $f_r = \alpha_0/(2d_0)$ and $k_0 = h_0\sqrt{\varepsilon_0/(z_0\alpha_0)}$ by using acoustic velocity α_0, thickness d_0, piezoelectric stress constant h_0, and dielectric permittivity ε_0 of the disk. Eq. (6) is symmetric with respect to source and receiver.

In order to derive H^a defined by Eq. (4), the transfer function between F^S and F^R_{inc} is calculated by considering the wave propagation in the sample. For simplicity, F^S is assumed to be uniform on the surface of the source transducer. F^R_{inc} is calculated as the average of the traction over the surface of the receiver transducer as

$$F^R_{\mathrm{inc}}(f) = F^S(f)\cdot\frac{1}{\pi a_0^2}\iint_{A^R}\iint_{A^S} g(f,\mathbf{x}-\mathbf{x}';v,Q)\,\mathrm{d}\mathbf{x}'\,\mathrm{d}\mathbf{x}, \tag{8}$$

where $g(f,\mathbf{x}-\mathbf{x}';v,Q)$ is the Green's function for a semi-infinite medium [17,18] with phase velocity $v(f)$ and quality factor $Q(f)$. A^S and A^R represent the surface of the source and receiver transducers, respectively, and $\mathbf{x}'$ and $\mathbf{x}$ represent points on A^S and A^R, respectively. The a_0 is the radius of the piezoelectric disk. By comparing Eqs. (8) and (4), H^a is obtained as

$$H^a(f) = \frac{1}{\pi a_0^2}\exp\left(\mathrm{i}\omega\frac{l}{v}\right)\exp\left(\frac{\omega l}{2vQ}\right)\iint_{A^{\mathrm{R}}}\iint_{A^{\mathrm{S}}} g(f,\mathbf{x}-\mathbf{x}';v,Q)\,\mathrm{d}\mathbf{x}\,\mathrm{d}\mathbf{x}'. \tag{9}$$

By calculating the integrals over A^S and A^R, we obtain

$$\begin{cases} H^a_P(f) = 2\exp\left(2\pi\mathrm{i}\dfrac{lf}{v_P}\right)\exp\left(\dfrac{\pi lf}{v_P Q_P}\right)\displaystyle\int_0^\infty \frac{w_P(f,p)}{p}\{J_1(p)\}^2\,\mathrm{d}p, \\ H^a_S(f) = 2\exp\left(2\pi\mathrm{i}\dfrac{lf}{v_S}\right)\exp\left(\dfrac{\pi lf}{v_S Q_S}\right)\displaystyle\int_0^\infty \frac{w_S(f,p)}{p}\{J_1(p)\}^2\,\mathrm{d}p, \end{cases} \tag{10}$$

where subscripts P and S represent longitudinal and shear waves, respectively, and $J_1(p)$ represents the Bessel function of the 1st order. Functions w_P and w_S are given by

$$\begin{cases} w_P(f,p) = \{-(2p^2-p_S^2)^2\mathrm{e}^{-\xi_P l/a_0} + 4\xi_P\xi_S p^2\mathrm{e}^{-\xi_S l/a_0}\}\Lambda^{-1}, \\ w_S(f,p) = \{4\xi_P\xi_S p^2\mathrm{e}^{-\xi_P l/a_0} - (2p^2-p_S^2)^2\mathrm{e}^{-\xi_S l/a_0}\}\Lambda^{-1}, \end{cases} \tag{11}$$

where

$$\begin{cases} \Lambda(f,p) = (2p^2-p_S^2)^2 - 4\xi_P\xi_S p^2, \\ \xi_P^2(f,p) = p^2 - p_P^2, \\ \xi_S^2(f,p) = p^2 - p_S^2, \end{cases} \tag{12}$$

in which both real and imaginary parts of ξ_P and ξ_S are taken to be positive, and

$$\begin{cases} p_P(f) = 2\pi\dfrac{a_0 f}{v_P}\left(1-\dfrac{\mathrm{i}}{2Q_P}\right), \\ p_S(f) = 2\pi\dfrac{a_0 f}{v_S}\left(1-\dfrac{\mathrm{i}}{2Q_S}\right). \end{cases} \tag{13}$$

2.2. Calculation of transducer effect H^T and diffraction effect H^a

2.2.1. Calculation of H^T

The broadband longitudinal and shear wave transducers used in the present experiments are V103 and V153, respectively, manufactured by Panametrics, inc. Values of f_r, k_0, Q_b, z_b/z_0, and z_s/z_0, which are needed to calculate H^T from Eq. (6), are listed in Table 1. Values of k_0, Q_b, and z_b/z_0, which are usually unknown, can be measured by using the direct contact method presented in Appendix B. Although Q_b determined from this method has a large uncertainty, the effect of Q_b on H^T is small, as shown below, and we can use $Q_b = 10$.

Table 1
Parameters used to calculate H^T and H^a for longitudinal and shear wave transducers.

	V103 (longitudinal)	V153 (shear)	Use
Transducer properties			
f_r (kHz)	1000	1000	H^T
a_0 (mm)	6.5	6.5	H^a
z_0 (10^7 kg m^{-2} s)	2.8	1.7	H^T
k_0	0.235[a]	0.224[a]	H^T
Q_b	10[a]	10[a]	H^T
z_b/z_0	1[a]	1[a]	H^T
Sample properties			
z_s (kg m^{-2} s)	$\rho \cdot v_P(f \geqslant f_r)$[b]	$\rho \cdot v_S(f \geqslant f_r)$[b]	H^T
v_P (km/s)	$v_P(f \geqslant f_r)$[c]	$v_S(f \geqslant f_r) \cdot \sqrt{3}$	H^a
v_S (km/s)	$v_P(f \geqslant f_r)/\sqrt{3}$	$v_S(f \geqslant f_r)$[c]	H^a
Q_P	10^4	1	H^a
Q_S	1	10^4	H^a
l (mm)	20–100	20–100	H^a

[a]The values were estimated by the direct contact method.
[b]$\rho \cdot v_P(f \geqslant f_r) = 4.5 \times 10^7$ kg m^{-2} s for stainless steel, 3.1×10^6 kg m^{-2} s for acrylic plastic, 1.8×10^6 kg m^{-2} s for the partially molten organic polycrystal, and $\rho \cdot v_S(f \geqslant f_r) = 1.9 \times 10^6$ kg m^{-2} s for acrylic plastic.
[c]$v_P(f \geqslant f_r) = 5.71$ km/s for stainless steel, 2.70 km/s for acrylic plastic, and 1.83 km/s for the partially molten organic polycrystal, and $v_S(f \geqslant f_r) = 1.38$ km/s for acrylic plastic.

The z_s is calculated by using a phase velocity at $f \geqslant f_r$. As shown in Section 2.3, a rough estimation of v at $f \geqslant f_r$ can be obtained from the raw data without correcting for H^T and H^a.

We express complex number H in terms of amplitude $A[H]$ and phase $P[H]$ as

$$H = A[H]\exp(\mathrm{i}P[H]), \tag{14}$$

where $A[H](>0)$ and $P[H]$ are real numbers. Fig. 2 shows $A[H^T]$ and $P[H^T]$ of V103 calculated for a stainless steel sample ($z_s/z_0 = 1.6$), an acrylic plastic sample ($z_s/z_0 = 0.11$), and an organic polycrystal sample ($z_s/z_0 = 0.065$). Although z_s/z_0 affects $A[H^T]$, it does not significantly affect $P[H^T]$ nor the frequency dependence of $A[H^T]$, which are important for the accurate estimation of $v(f)$ and $Q(f)$. This result indicates the validity to calculate z_s by using a rough estimation of v at $f \geqslant f_r$. Also shown in Fig. 2 are $A[H^T]$ and $P[H^T]$ of V103 calculated for various values of sample quality factor Q and backing quality factor Q_b. Although $Q = \infty$ is assumed in deriving Eq. (6), effects of Q can be investigated by replacing z_s in Eq. (6) by $z_s\{1 - \mathrm{i}/(2Q)\}$. Fig. 2 shows that the effects of Q on H^T are negligibly small, and hence shows the validity to use $Q = \infty$ regardless of an actual value of Q. Fig. 2 also shows that effects of Q_b on H^T are small, and hence shows the validity to use $Q_b = 10$.

At $z_b/z_0 \simeq 1$, the asymptotic form of Eq. (6) at $f \to 0$ is obtained as

$$\begin{cases} A[H^T] = 2\pi k_0^2 \dfrac{z_s/z_0}{(1 + z_s/z_0)^2} \dfrac{f}{f_r} \\ P[H^T] = \dfrac{\pi}{2}\left(1 - 2\dfrac{f}{f_r}\right) \end{cases} \quad (f \ll f_r \quad \text{and} \quad z_b/z_0 \simeq 1). \tag{15}$$

The most important feature of H^T is that $P[H^T]$ approaches $\pi/2$ at $f \to 0$. Because the correction of traveltime for the transducer effect is given by $P[H^T]/\omega$, that $P[H^T]$ is not equal to 0 at $f \to 0$ indicates the significance of the correction for H^T at low frequency.

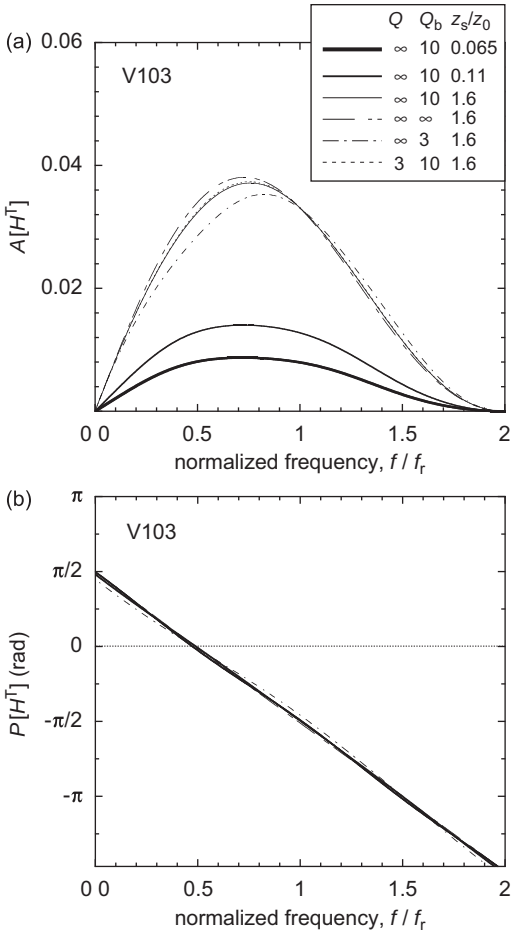

Fig. 2. Transducer effect H^T of broadband longitudinal transducer V103 calculated for various values of Q, Q_b, and z_s/z_0. (a) Amplitude $A[H^T]$ and (b) phase $P[H^T]$.

2.2.2. Calculation of H^a

Values of l, a_0, v_P, Q_P, v_S, and Q_S, which are needed to calculate H^a from Eq. (10), are listed in Table 1. The values of v_P and v_S used to calculate H_P^a and H_S^a, respectively, are roughly estimated by the phase velocities at $f \geqslant f_r$ without correcting for H^T and H^a. By using these v_P and v_S, v_S and v_P used to calculate H_P^a and H_S^a, respectively, are estimated by assuming $v_P/v_S = \sqrt{3}$. $(Q_P, Q_S) = (10^4, 1)$ for H_P^a and $(Q_P, Q_S) = (1, 10^4)$ for H_S^a are used regardless of the actual values of Q_P and Q_S. The validity of these assumptions is discussed later. The integral in Eq. (10) is calculated numerically.

Fig. 3 shows H_P^a of V103 calculated for $l = 100$, 50, and 20 mm samples. The value of v_P controls H_P^a through only the normalized frequency $(a_0/v_P)f$, and also the value of v_S controls H_S^a through only $(a_0/v_S)f$. Each symbol in Fig. 3 shows the transition point from point source to infinite size source, where the frequency is given by

$$f = \frac{v_i}{2(\sqrt{l^2 + 4a_0^2} - l)} \quad (i = P, S). \tag{16}$$

At this frequency, the difference between the longest and the shortest paths from the source to the receiver is equal to the half wavelength (Fig. 4). Note that Eq. (16) is obtained for finite size source and finite size receiver. The distance l obtained from Eq. (16) is different from the well-known Fresnel distance, which is derived for finite size source and point receiver (Fig. 4). When l is large, the asymptotic form of H_P^a and H_S^a at

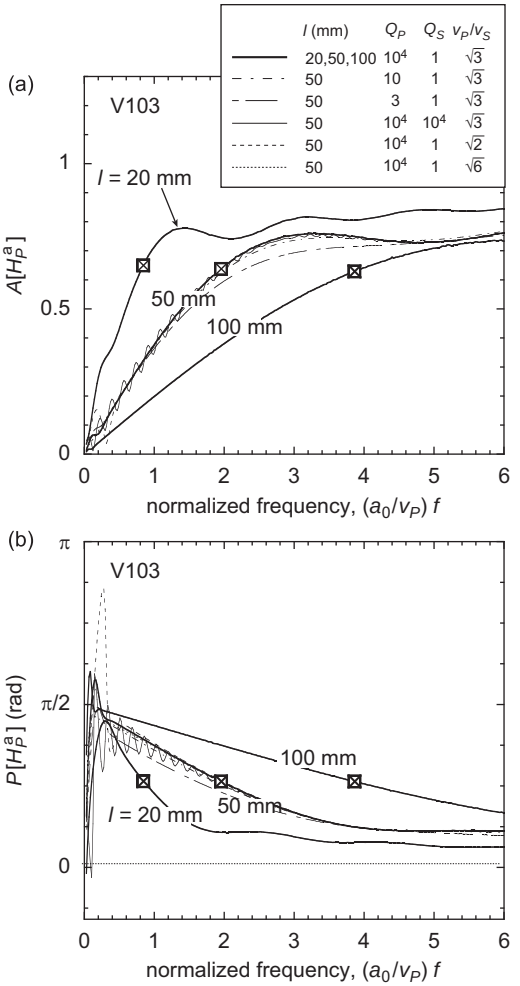

Fig. 3. Diffraction effect H_P^a of longitudinal transducer V103 calculated for various values of l, Q_P, Q_S, and v_P/v_S. (a) Amplitude $A[H_P^a]$ and (b) phase $P[H_P^a]$. Symbols show the transition point from point source to infinite size source.

$f \to 0$ is written as

$$\begin{cases} A[H_i^a] = \dfrac{\pi a_0^2 f}{l v_i} \\ P[H_i^a] = \dfrac{\pi}{2} \end{cases} \quad \left(2\pi \frac{a_0 f}{v_i} \ll 1 \quad \text{and} \quad l > \frac{v_i}{f},\ i = P, S \right) \tag{17}$$

(Appendix C), which represents the far-field wave excited by a point source. $P[H^a]$ approaches $\pi/2$ at $f \to 0$. Hence, the correction of traveltime for H^a, $P[H^a]/\omega$, becomes very important at small f.

Fig. 3 also shows H_P^a of V103 calculated for various values of Q_P, Q_S, and v_P/v_S. The effect of Q_P on H_P^a is small, indicating the validity to use $Q_P = 10^4$ without knowing the actual value of Q_P. Although the effect of Q_S on H_P^a is small, when Q_S is large, $A[H_P^a]$ and $P[H_P^a]$ fluctuate rapidly at $(a_0/v_P)f < 3$. This fluctuation is difficult to measure accurately in the experiments, and the use of such H_P^a in data analysis may cause artificial noise. Therefore, $Q_S = 1$ should be used to remove the fluctuation. The effect of v_P/v_S is small except for $(a_0/v_P)f \ll 1$, indicating the validity to use $v_P/v_S = \sqrt{3}$. In the same manner, $Q_S = 10^4$, $Q_P = 1$, and $v_P/v_S = \sqrt{3}$ are used for calculating H_S^a.

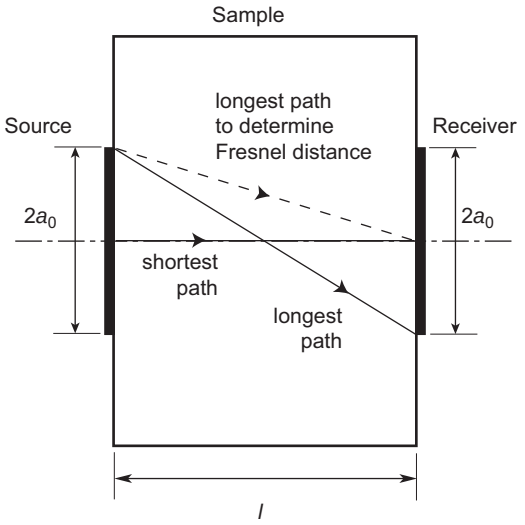

Fig. 4. The longest and the shortest paths between source and receiver transducers. The longest path is longer than that used in the evaluation of Fresnel distance (dotted line).

2.3. Estimation of v and Q from H^{obs}

By using H^T and H^a obtained in the previous sections, $v(f)$ and $Q(f)$ can be calculated from H^{obs} as

$$\frac{l}{v(f)} = \frac{1}{\omega}(-P[H^{\mathrm{obs}}] + 2\pi n + P[H^T] + P[H^a]), \tag{18}$$

$$\exp\left(-\frac{\pi f l}{v(f)Q(f)}\right) = \frac{A[H^{\mathrm{obs}}]}{A[H^T]A[H^a]}. \tag{19}$$

$P[H^{\mathrm{obs}}]$ is defined as a continuous function of f over the experimental frequency range, and hence is not limited to 0–(-2π). $P[H^{\mathrm{obs}}]$ has an uncertainty of $2\pi n$ with integer n, which is explicitly shown in Eq. (18). The results of Section 2.2 show that $P[H^T]$ and $P[H^a]$ approach $\pi/2$ at $f \to 0$. Hence, n can be determined from the requirement of

$$-P[H^{\mathrm{obs}}] + 2\pi n + \pi = 0 \quad \text{at } f = 0. \tag{20}$$

Even when the data are obtained by using sinusoidal waves, and hence n is completely unknown, n can be determined by Eq. (20).

At $f \simeq f_r$ (1 MHz), $|P[H^T]|$ and $|P[H^a]|$ are, respectively, nearly equal to and less than $\pi/2$ (Figs. 2 and 3). Hence, the effects of $P[H^T]$ and $P[H^a]$ on the traveltimes are, respectively, nearly equal to and less than $1/(4f_r)$, which are much smaller than the traveltimes obtained in the present experiments. Hence, $v(f \geqslant f_r)$ can be accurately estimated from $(-P[H^{\mathrm{obs}}] + 2\pi n)$, without correcting for H^T and H^a.

3. Experiments

3.1. Data before correction

By using the assembly shown in Fig. 1, $V^S(f)$ and $V^R(f)$ were measured for $f = 100\,\mathrm{kHz}-1\,\mathrm{MHz}$. A stainless steel sample with $l = 50\,\mathrm{mm}$, acrylic plastic samples with $l = 50$ and $100\,\mathrm{mm}$, and a partially molten organic polycrystal sample with $l = 20\,\mathrm{mm}$ were used. The measurements were made using two types of waves: sinusoidal wave and narrow band pulse. With the sinusoidal wave with frequency f, $A[H^{\mathrm{obs}}(f)]$ and $P[H^{\mathrm{obs}}(f)]$ are obtained immediately from the amplitude ratio and phase difference, respectively, between $V^S(t)$ and

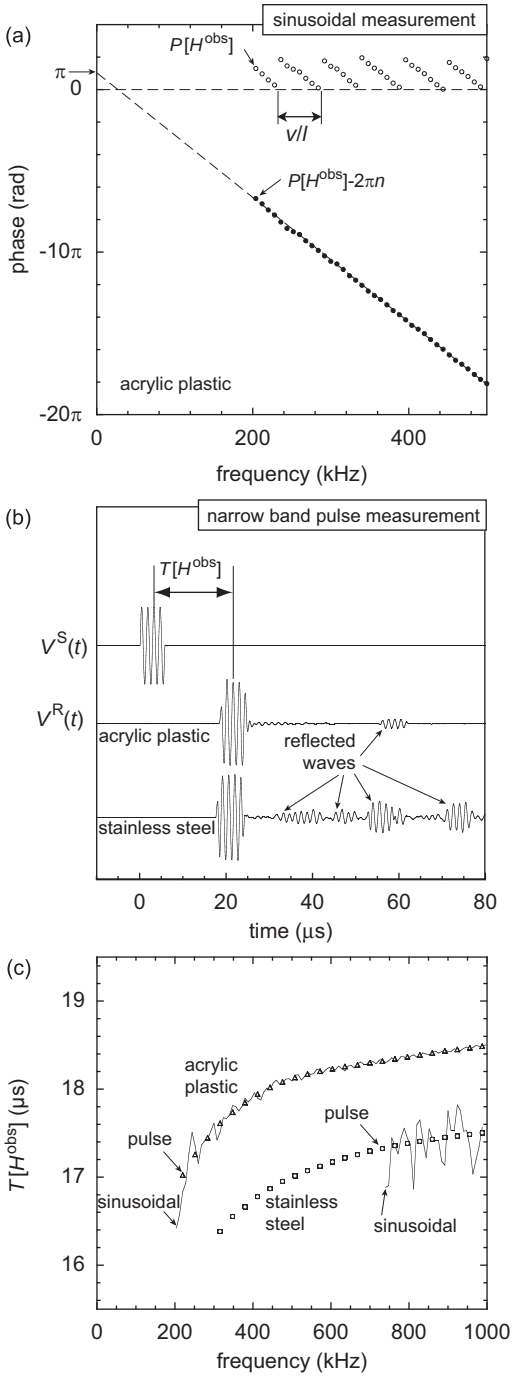

Fig. 5. Procedures to determine traveltime for the acrylic plastic sample with $l = 50$ mm and the stainless steel sample with $l = 100$ mm. (a) Phase data from sinusoidal measurement. From the phase delay data between $V^R(t)$ and $V^S(t)$ ($P[H^{obs}]$, open symbols), continuous function ($P[H^{obs}] - 2\pi n$, solid symbols) is obtained, where n is determined to satisfy Eq. (20). Only the data for the acrylic plastic sample are shown. (b) Waveform data from narrow band pulse measurement. Traveltime $T[H^{obs}]$ is read as the time difference of the 3rd peaks of $V^R(t)$ and $V^S(t)$. (c) Traveltime $T[H^{obs}]$ obtained from sinusoidal measurement (lines) and narrow band pulse measurement (symbols).

$V^R(t)$. Solid symbols in Fig. 5(a) show $P[H^{obs}] - 2\pi n$, where n was determined to satisfy Eq. (20). In order to construct $P[H^{obs}]$ correctly from the measured phase difference (open symbols in Fig. 5(a)), frequency step Δf should satisfy $\Delta f \ll v/l$. With the narrow band pulse with cycle frequency f, traveltime at frequency f was

determined as the time difference of the 3rd peak between $V^S(t)$ and $V^R(t)$ (Fig. 5(b)). Also, after removing the reflected waves from $V^R(t)$, the Fourier coefficient $V^R(f)$ was calculated, and $A[H^{\mathrm{obs}}(f)]$ was determined as the amplitude ratio between $V^R(f)$ and $V^S(f)$. Unlike the sinusoidal measurement, narrow band pulse measurement does not have any limitation on the frequency step.

Using $P[H^{\mathrm{obs}}] - 2\pi n$ obtained from the sinusoidal waves, uncorrected traveltime $T[H^{\mathrm{obs}}]$ is calculated by

$$T[H^{\mathrm{obs}}] = -\frac{1}{\omega}(P[H^{\mathrm{obs}}] - 2\pi n). \tag{21}$$

The results are shown in Fig. 5(c) (lines) together with the traveltimes obtained from the narrow band pulses (symbols). For the acrylic plastic sample, the two results agree well, indicating the validity of both measurements. For the stainless steel sample, however, both results do not agree. The result of the sinusoidal measurement shows a rapid fluctuation with f. This fluctuation is caused by the reflected waves, which have large amplitude because of the high Q of the sample (Fig. 5(b)). Such fluctuation does not occur in the result of the narrow band pulse measurement, which are not affected by the reflected waves. The narrow band pulse measurement is therefore applicable to both high-Q and low-Q samples.

3.2. Estimation of frequency dependent phase velocity and quality factor

H^{obs} obtained from the sinusoidal and narrow band pulse measurements is corrected for H^T and H^a as Eqs. (18) and (19). Phase velocity and amplitude obtained after the corrections are shown in Fig. 6, together with those without the corrections. Also shown in Fig. 6 are dispersion and amplitude theoretically predicted from the constant-Q model [19] (dashed lines). Without the corrections, the results significantly deviate from the theoretical predictions. After the corrections, however, the results show good agreement with the theoretical predictions. These results demonstrate the validity of the present corrections by using the

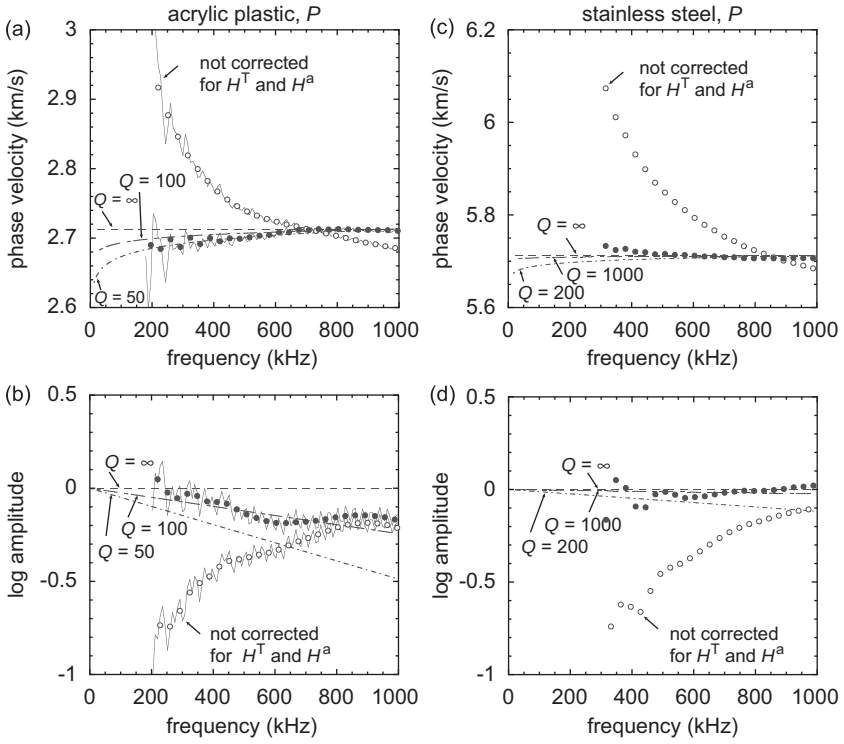

Fig. 6. (a) Phase velocity and (b) amplitude of longitudinal wave for the acrylic plastic sample measured by using sinusoidal waves (lines) and narrow band pulses (symbols). (c) Phase velocity and (d) amplitude of longitudinal wave for the stainless steel sample measured by narrow band pulse (symbols). Results before and after the corrections for H^T and H^a are shown. Dashed lines show theoretical predictions from the constant-Q model. The results after the corrections agree well with the model predictions.

theoretically calculated H^T and H^a. The corrections are significant at low frequencies (f lower than the resonant frequency f_r and lower than the transition frequency given by Eq. (16)). Note that the phase velocity (Fig. 6(a) and (c)) and the amplitude (Fig. 6(b) and (d)) are obtained from $P[H^{\mathrm{obs}}]$ and $A[H^{\mathrm{obs}}]$, respectively, and hence are obtained independently from each other. The estimate of $Q \gg 200$ for the stainless steel sample and $100 > Q > 50$ for the acrylic plastic sample, which are obtained consistently from both phase velocity and amplitude, confirm the validity of the present method. Fig. 7 shows the phase velocity and amplitude of longitudinal and shear waves obtained for the acrylic plastic samples with $l = 50$ and 100 mm. Nearly constant Q ($Q_P = 80$ and $Q_S = 80$) is obtained consistently for both $l = 50$ and 100 mm samples.

Phase velocity and quality factor obtained for the partially molten organic polycrystal sample are shown in Fig. 8. This sample is a binary eutectic system composed of borneol and diphenylamine [20], and the partially molten state was achieved at 60 °C. Because Q is very low, only the direct wave propagated through the sample can be observed. Hence, the existing method to eliminate the transducer effect using reflected waves cannot be applied to this sample. By using the method developed in this study, $Q = 4$ was determined consistently from both phase velocity and amplitude.

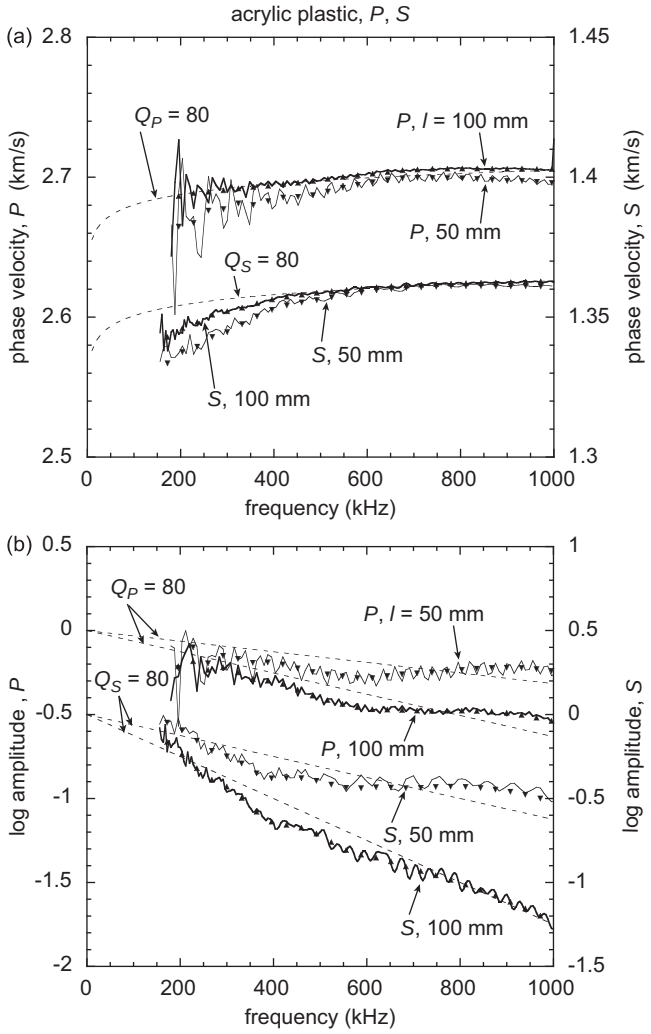

Fig. 7. (a) Phase velocity and (b) amplitude of longitudinal wave (P) and shear wave (S) for acrylic plastic samples with $l = 50$ and 100 mm. Solid lines show the data obtained by sinusoidal waves, and the symbols show the data obtained by narrow band pulses. Dashed lines show the predictions from the constant-Q model with $Q_P = 80$ and $Q_S = 80$.

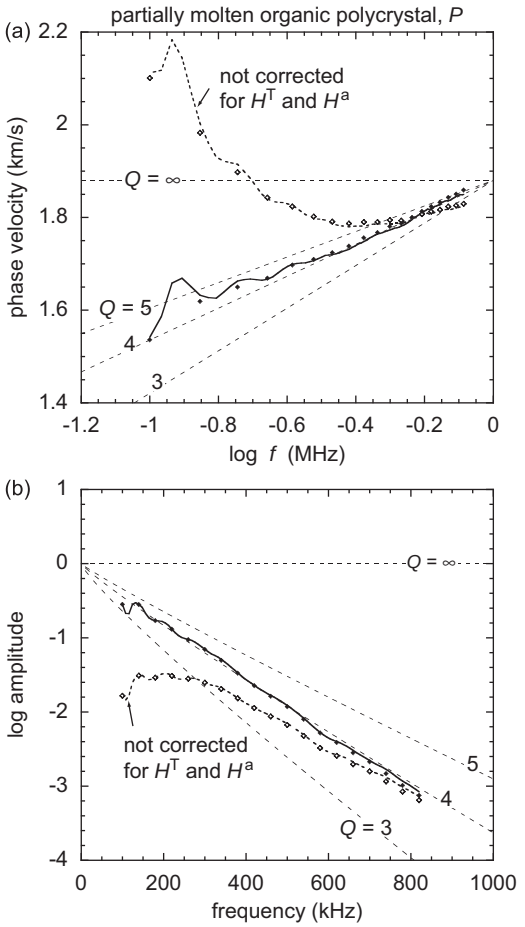

Fig. 8. (a) Phase velocity and (b) amplitude of longitudinal wave for the partially molten organic polycrystal sample measured by using sinusoidal waves (lines) and narrow band pulses (symbols). Results before and after the corrections for H^T and H^a are shown. Thin dashed lines show the theoretical predictions from the constant-Q model.

3.3. A brief discussion on the reference method

Let $H^{\mathrm{obs}}_{\mathrm{ref}}(f)$ be the transfer function $H^{\mathrm{obs}}(f)$ of a reference sample with phase velocity v_{ref}, quality factor Q_{ref}, and sample length l_{ref}. The deconvolved spectrum between $H^{\mathrm{obs}}(f)$ and $H^{\mathrm{obs}}_{\mathrm{ref}}(f)$ is written as

$$\frac{H^{\mathrm{obs}}}{H^{\mathrm{obs}}_{\mathrm{ref}}}=\frac{H^T}{H^T_{\mathrm{ref}}}\frac{H^a}{H^a_{\mathrm{ref}}}\exp\left\{-\mathrm{i}\omega\left(\frac{l}{v}-\frac{l_{\mathrm{ref}}}{v_{\mathrm{ref}}}\right)\right\}\exp\left\{-\frac{\omega}{2}\left(\frac{l}{vQ}-\frac{l_{\mathrm{ref}}}{v_{\mathrm{ref}}Q_{\mathrm{ref}}}\right)\right\}, \tag{22}$$

where H^T_{ref} and H^a_{ref} represent H^T and H^a, respectively, for the reference sample. In the reference methods, v and Q are estimated from $H^{\mathrm{obs}}/H^{\mathrm{obs}}_{\mathrm{ref}}$ by assuming $H^T/H^T_{\mathrm{ref}}=H^a/H^a_{\mathrm{ref}}=1$. The results in Section 2 show that $H^T(f)/H^T_{\mathrm{ref}}(f)=1$ is valid if $v_{\mathrm{ref}}=v$ and $l_{\mathrm{ref}}=l$. If $v\neq v_{\mathrm{ref}}$ and/or $l\neq l_{\mathrm{ref}}$, H^a/H^a_{ref} deviates from unity, especially at frequencies lower than the transition frequency given by Eq. (16). Fig. 9 shows phase velocity and amplitude obtained from this study (solid lines), and those which are obtained with the reference method (dotted bold lines). $H^{\mathrm{obs}}_{\mathrm{ref}}$ is not measured but is derived theoretically by calculating H^a_{ref} and H^T_{ref} for water ($v_{\mathrm{ref}}=1.50\,\mathrm{km\,s^{-1}}$, $Q_{\mathrm{ref}}=\infty$) or acrylic plastic ($v_{\mathrm{ref}}=2.70\,\mathrm{km\,s^{-1}}$, $Q_{\mathrm{ref}}=80$) with $l_{\mathrm{ref}}=l$. The accuracy of the reference method decreases as the difference between v and v_{ref} increases. Because it is practically difficult to find a reference sample satisfying $v_{\mathrm{ref}}=v$, the present method applicable to general materials is useful.

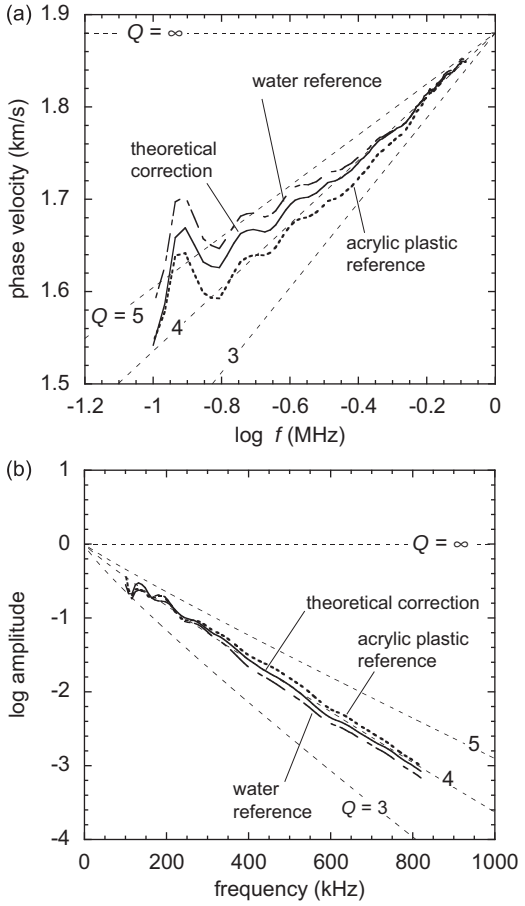

Fig. 9. (a) Phase velocity and (b) amplitude of longitudinal wave for the partially molten organic polycrystal sample. Bold solid lines show the results obtained from the present method and the bold dashed lines show the results which are to be obtained from the reference method by using water and acrylic plastic samples. Thin dashed lines show the predictions from the constant-Q model.

4. Conclusions

We have developed a new method to determine frequency dependent phase velocity and quality factor from ultrasonic wave transmission. In this method, the transducer effect H^T and the diffraction effect H^a, for which the waveform data must be corrected, are calculated theoretically without using any reference sample. We also developed several practical methods to estimate the material properties needed for the calculation of H^T and H^a. The phase of H^T and that of H^a approach $\pi/2$ at $f \to 0$, and hence the corrections are significant at low frequencies. Using the present method, we demonstrated Q for a stainless steel sample ($Q_P \gg 200$), acrylic plastic samples ($Q_P = 80$, $Q_S = 80$), and a partially molten organic polycrystal sample ($Q_P \simeq 4$) for 100 kHz–1 MHz. The present method is applicable to general materials. Validity and limitation of the previous method based on the reference waveform were discussed.

Acknowledgment

The authors would like to thank T.L. Wright and B.K. Holtzman for checking the English of this manuscript.

Appendix A. Detailed formulation for the dynamic response of transducers

We consider a broadband transducer consisting of a piezoelectric disk and a backing (Fig. 10). The disk has radius a_0, thickness d_0, density ρ_0, acoustic velocity α_0, acoustic impedance $z_0 = \rho_0\alpha_0$, dielectric permittivity ε_0, and piezoelectric stress constant h_0, which represents the stress caused by a unit electric displacement. V (V) and I (A) denote the voltage difference and current, respectively, between the two electrodes. F (Pa) and u ($\mathrm{m\,s^{-1}}$) represent traction and velocity, respectively, of the disk at the sample side, and F_b and u_b represent those at the backing side. These F, u, F_b, and u_b represent the normal components (outward positive) for a longitudinal wave transducer, and the tangential components for a shear wave transducer. Although source and receiver transducers have the same material parameters, the two transducers are used under different electrical boundary conditions, and hence should be treated separately.

We first consider a source transducer, which is denoted by superscript S. By solving the mechanical and electrical governing equations for the disk [14], we obtain

$$\begin{pmatrix} F^S \\ F_b^S \\ \frac{h_0}{\mathrm{i}\omega\pi a_0^2} I^S \end{pmatrix} = z_0 \begin{pmatrix} D^S & C^S & -\mathrm{i}\varepsilon \\ C^S & D^S & -\mathrm{i}\varepsilon \\ -\mathrm{i}\varepsilon & -\mathrm{i}\varepsilon & \mathrm{i}\varepsilon \end{pmatrix} \begin{pmatrix} u^S \\ u_b^S \\ \frac{\mathrm{i}\omega}{h_0} V^S \end{pmatrix} \tag{A.1}$$

in the frequency domain, where ε, D^S, and C^S are given by Eq. (7) in the text. The boundary conditions are given by

$$\frac{F^S}{u^S} = -z_s, \tag{A.2}$$

$$\frac{F_b^S}{u_b^S} = -z_b\left(1 - \frac{\mathrm{i}}{2Q_b}\right), \tag{A.3}$$

where z_b is the real part of the acoustic impedance of the backing, Q_b the quality factor of the backing, and z_s the acoustic impedance of the sample [14]. As shown in Section 2.2.1, imaginary part of z_s can be neglected.

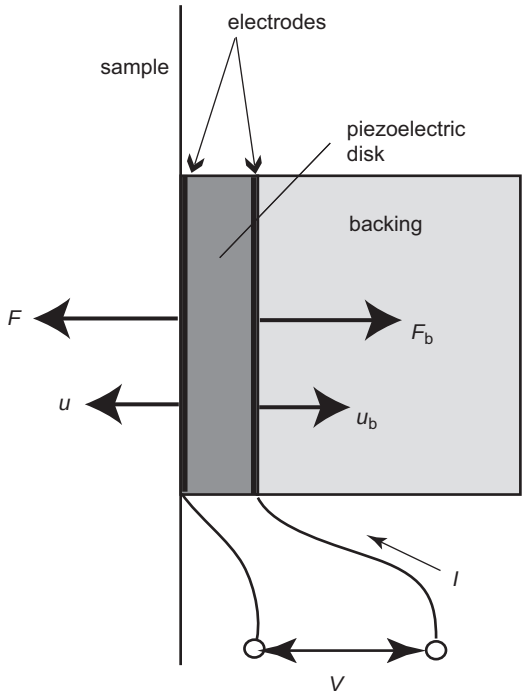

Fig. 10. Schematic illustration of a broadband transducer consisting of piezoelectric disk and backing.

The same relation as Eq. (A.1) is also required for the receiver transducer. The receiver transducer is denoted by superscript R. Since V^R is measured by an oscilloscope with high input impedance, the condition $I^R = 0$ is required. Then, Eq. (A.1) can be written as

$$\begin{pmatrix} F^R \\ F_b^R \\ z_0 \cdot \dfrac{\mathrm{i}\omega}{h_0} V^R \end{pmatrix} = z_0 \begin{pmatrix} D^R & C^R \\ C^R & D^R \\ 1 & 1 \end{pmatrix} \begin{pmatrix} u^R \\ u_b^R \end{pmatrix}, \tag{A.4}$$

where D^R and C^R are given by Eq. (7) in the text. The boundary condition on the backing side is given by

$$\frac{F_b^{\mathrm{R}}}{u_b^{\mathrm{R}}} = -z_b \left(1 - \frac{\mathrm{i}}{2Q_b}\right). \tag{A.5}$$

From Eqs. (A.4) and (A.5), we obtain

$$\frac{F^R}{u^R} = z_s \left\{ D^R + \frac{(C^R)^2}{(z_b/z_0)(1 - \mathrm{i}/(2Q_b)) - D^R} \right\} = -z^R. \tag{A.6}$$

Note the difference between Eqs. (A.6) and (A.2). While F^S/u^S is equal to the sample impedance z_s, F^R/u^R is not equal to z_s. Therefore, F^R and u^R consist of not only the traction and velocity, respectively, of incident wave but also those of reflected wave. Let F^R_{inc} be the traction of incident wave. From the continuity of both stress and velocity at the interface, the relation between F^R and F^R_{inc} is obtained as

$$\frac{F^R}{F^R_{\mathrm{inc}}} = \frac{2z^R}{z_s + z^R}, \tag{A.7}$$

where z^R is defined by Eq. (A.6). Transducer effect H^T is obtained by solving Eqs. (A.1)–(A.7.).

Appendix B. Direct contact method

Let $H^D(f)$ be the ratio of the output voltage $V^R(f)$ to the input voltage $V^S(f)$ obtained from the receiver and source transducers, respectively, directly contacted without a sample. The values of k_0, Q_b, and z_b/z_0, which are needed to calculate H^T, can be determined by comparing the measured and predicted H^D. The governing equations are given by Eqs. (A.1) and (A.4). The boundary conditions on the backing side are given by Eqs. (A.3) and (A.5), and those on the other side are given by

$$\begin{cases} F^S = F^R, \\ u^S = -u^R. \end{cases} \tag{B. 1}$$

Then, H^D is solved as

$$\begin{aligned} H^D = {} & \frac{k_0^2}{\pi(f/f_r)} \{(z_b/z_0)(1 - \mathrm{i}/(2Q_b)) - D^S + C^S\} \\ & \times \{(z_b/z_0)(1 - \mathrm{i}/(2Q_b)) - D^R + C^R\} \\ & \times ((D^S + D^R)\{(z_b/z_0)(1 - \mathrm{i}/(2Q_b)) - D^S\} \\ & \times \{(z_b/z_0)(1 - \mathrm{i}/(2Q_b)) - D^R\} \\ & + (C^S)^2\{(z_b/z_0)(1 - \mathrm{i}/(2Q_b)) - (D^S)^2\} \\ & + (C^R)^2\{(z_b/z_0)(1 - \mathrm{i}/(2Q_b)) - (D^R)^2\})^{-1}. \end{aligned} \tag{B. 2}$$

Symbols in Fig. 11 show H^D experimentally measured for the longitudinal transducers V103. Also shown in Fig. 11 are the theoretical predictions calculated by using Eq. (B. 2) for various values of z_b/z_0 and Q_b (lines). The acoustic impedance of the backing relative to that of the piezoelectric disk, z_b/z_0, controls the intensity of the resonance. When z_b/z_0 is much smaller than or larger than unity, the resonance is strong and $A[H^D]$ has a

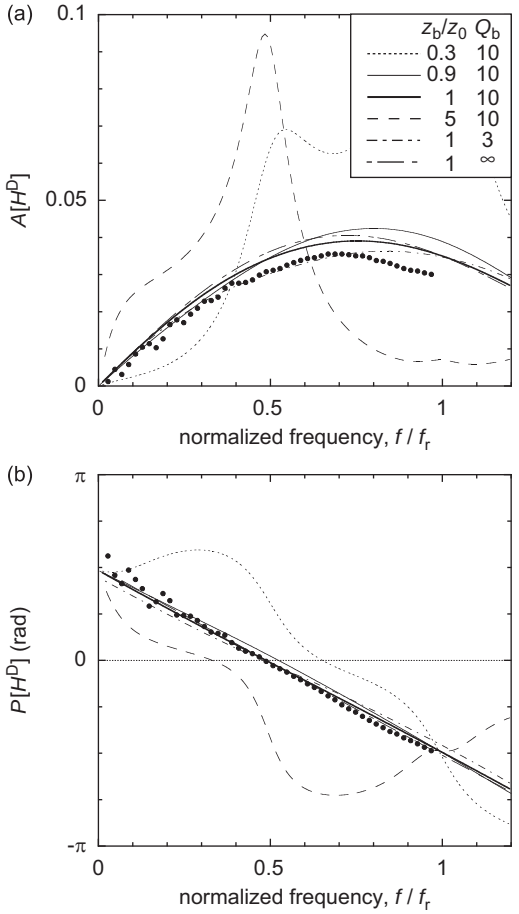

Fig. 11. Transfer function H^D obtained by directly contacting two longitudinal transducers V103. (a) Amplitude $A[H^D]$ and (b) phase $P[H^D]$. Symbols show the experimental data, and lines show the theoretical predictions calculated for various values of z_b/z_0 and Q_b.

sharp peak. When z_b/z_0 is close to unity, $A[H^D]$ shows a broad peak and $P[H^D]$ shows a monotonic decrease. The experimental data are explained well by $z_b/z_0 = 1$. The effect of Q_b on H^D is small, and hence Q_b cannot be determined uniquely. As shown in Section 2.2.1, the effect of Q_b on H^T is small and hence we can use $Q_b = 10$. $A[H^D]$ is proportional to k_0^2. Best fit for V103 and V153 are obtained at $k_0 = 0.235$ and 0.224, respectively.

Appendix C. Asymptotic form of H^a

At the limit of $f \to 0$, $|p_i| \ll 1$ $(i = P, S)$. For $0 \leqslant p \leqslant p_i$, ξ_i is an imaginary number, and w_i given by Eq. (11) is approximated as $w_i \simeq \{1 + O(p^2)\} \exp(-\xi_i l/a_0)$. For $p > p_i$, ξ_i is a real number, and w_i exponentially decreases with increasing p. When $l > v_i/f$, the decrease is very rapid and the integral for $p > p_i$ is negligible. Therefore, H^a is approximated as

$$\begin{aligned} H_i^a &\simeq 2\exp\left(-2\pi \mathrm{i}\frac{lf}{v_i}\right)\int_0^{p_i}\frac{\exp(-\xi_i l/a_0)}{p}\{J_1(p)\}^2\,\mathrm{d}p \quad (i = P, S) \\ &\simeq \frac{1}{2}\exp\left(-2\pi \mathrm{i}\frac{lf}{v_i}\right)\int_0^{p_i} p\exp(-\xi_i l/a_0)\,\mathrm{d}p \\ &= \frac{\mathrm{i}\pi a_0^2 f}{l v_i} + O(l^{-2}), \end{aligned} \tag{C. 1}$$

which gives Eq. (17).

References

[1] Z.E.A. Fellah, F.G. Mitri, M. Fellah, E. Ogam, C. Depollier, Ultrasonic characterization of porous absorbing materials: Inverse problem, *Journal of Sound and Vibration* 302 (2007) 746–759.

[2] F.D. Denia, A. Selamet, F.J. Fuenmayor, R. Kirby, Acoustic attenuation performance of perforated dissipative mufflers with empty inlet/outlet extensions, *Journal of Sound and Vibration* 302 (2007) 1000–1017.

[3] T.J. Shankland, P.A. Johnson, T.M. Hopson, Elastic wave attenuation and velocity on Berea sandstone measured in the frequency domain, *Geophysical Research Letters* 20 (1993) 391–393.

[4] S.I. Rokhlin, D.K. Lewis, G.F. Graff, L. Adler, Real-time study of frequency dependence of attenuation and velocity of ultrasonic waves during the curing reaction of epoxy resin, *Journal of the Acoustical Society of America* 79 (1986) 1786–1793.

[5] N. Yoshioka, K. Iwase, A laboratory experiment to monitor the contact state of a fault by transmission wave, *Tectonophysics* 413 (2006) 221–238.

[6] A. Ribodetti, S. Operto, J. Virieux, G. Lambare, H.P. Valero, D. Givert, Asymptotic viscoacoustic diffraction tomography of ultrasonic laboratory data: a tool for rock properties analysis, *Geophysical Journal of International* 140 (2000) 324–340.

[7] E.P. Papadakis, K.A. Fowler, L.C. Lynnworth, Ultrasonic attenuation by spectrum analysis of pulses in buffer rods: method and diffraction corrections, *Journal of the Acoustical Society of America* 53 (1973) 1336–1343.

[8] H. Niesler, I. Jackson, Pressure derivatives of elastic wave velocities from ultrasonic interferometric measurements on jacketed polycrystals, *Journal of the Acoustical Society of America* 86 (1989) 1573–1585.

[9] J. Kushibiki, R. Okabe, M. Arakawa, Precise measurements of bulk-wave ultrasonic velocity dispersion and attenuation in solid materials in VHF range, *Journal of the Acoustical Society of America* 113 (2003) 3171–3178.

[10] J. Mobley, K.R. Waters, C.S. Hall, J.N. Marsh, M.S. Hughes, G.H. Brandenburger, J.G. Miller, Measurements and predictions of the phase velocity and attenuation coefficient in suspensions of elastic microspheres, *Journal of the Acoustical Society of America* 106 (1999) 652–659.

[11] A.N. Kalashnikov, R.E. Challis, Errors and uncertainties in the measurement of ultrasonic wave attenuation and phase velocity, *IEEE Transactions on Ultrasonics, Ferroelectrics, and Frequency Control* 52 (2005) 1754–1768.

[12] J.A. Donald, S.D. Butt, Experimental technique for measuring phase velocities during triaxial compression test, *International Journal of Rock Mechanics and Mining Science* 42 (2005) 307–314.

[13] P.R. Stepanishen, Pulsed transmit/receive response of ultrasonic piezoelectric transducers, *Journal of the Acoustical Society of America* 69 (1981) 1815–1827.

[14] W.P. Mason, *Physical Acoustics, Vol. 1*, Academic Press, New York, 1964.

[15] H. Seki, A. Granato, R. Truell, Diffraction effects in the ultrasonic fields of point source and their importance in the accurate measurement of attenuation, *Journal of the Acoustical Society of America* 28 (1956) 230–238.

[16] D.L. Anderson, *Theory of the Earth*, Blackwell Scientific Publications, 1989.

[17] K. Sezawa, Further studies on Rayleigh-waves having some azimuthal distribution, *Bulletin of Earthquake Research Institute* 6 (1929) 1–18.

[18] D.H. Ha, H. Higashihara, Wave field generated by laterally vibrating source attached to the surface of elastic half space, *Journal of Structure and Mechanics of Earthquake Engineering* 15 (1998) 1–10.

[19] H.P. Liu, D.L. Anderson, H. Kanamori, Velocity dispersion due to an elasticity; implications for seismology and mantle composition, *Geophysical Journal of Royal astronomical Society* 47 (1976) 41–58.

[20] Y. Takei, Acoustic properties of partially molten media studied on a simple binary system with a controllable dihedral angle, *Journal of Geophysical Research* 105 (2000) 16665–16682.